Front. Phys. 16(1), 12501 (2021)
https://doi.org/10.1007/s11467-020-0995-z

RESEARCH ARTICLE

Giant enhancement of photoluminescence emission in monolayer WS_2 by femtosecond laser irradiation

Cheng-Bing Qin,[1,2,†] Xi-Long Liang,[1,2] Shuang-Ping Han,[1,2] Guo-Feng Zhang,[1,2] Rui-Yun Chen,[1,2] Jian-Yong Hu,[1,2] Lian-Tuan Xiao,[1,2*] Suo-Tang Jia[1,2]

[1] *State Key Laboratory of Quantum Optics and Quantum Optics Devices, Institute of Laser Spectroscopy, Shanxi University, Taiyuan 030006, China*

[2] *Collaborative Innovation Center of Extreme Optics, Shanxi University, Taiyuan 030006, China*

Corresponding authors. E-mail: †chbqin@sxu.edu.cn, ‡xlt@sxu.edu.cn

Received August 3, 2020; accepted September 7, 2020

Supplementary Materials

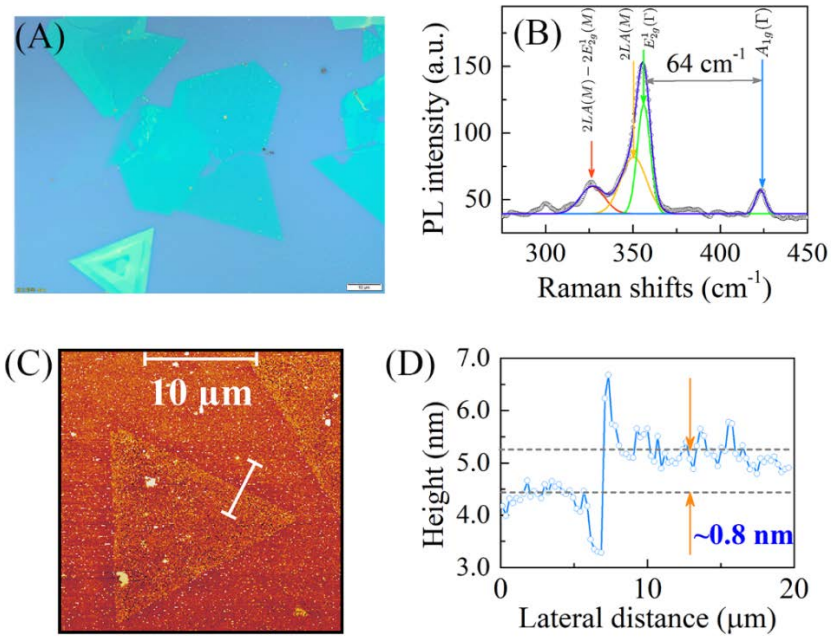

Fig. S1 Characterizations of the as-prepared sample. Optical image (A) and Raman spectroscopy (B) of monolayer WS_2 prepared by chemical vapor deposition (CVD). Raman spectroscopy are deconvoluted into four components with peak positions at 326.7 cm^{-1}, 351.4 cm^{-1}, 355.2 cm^{-1}, and 423.1 cm^{-1}, respectively. They can be attributed to the 2*LA*(M)-$2E^1_{2g}$(M), 2*LA*(M), E^1_{2g}(Γ), and A_{1g}(Γ), respectively, where E^1_{2g}(Γ), and A_{1g}(Γ) are the first order of the in-plane and out-of-plane modes, 2*LA*(M) and $2E^1_{2g}$(M) are the second-order longitudinal acoustic phonon and second-order in-plane modes near the M point of the Brillouin zone [1-3]. (C) Atomic force microscope (AFM) image and (D) the corresponding height profile along the line in C.

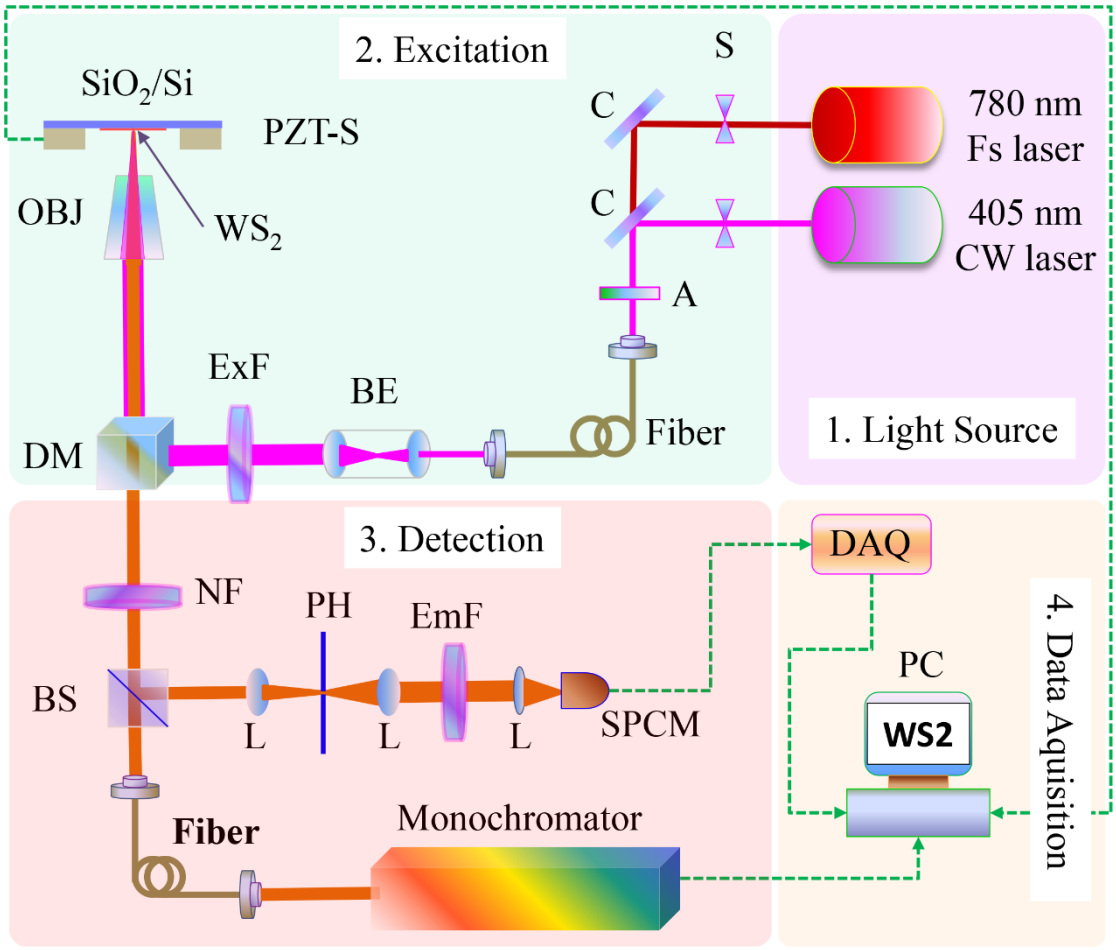

Fig. S2 Schematic diagram of the optical setup. S: shutter; C: beam combiner; A: attenuator; BE: beam expander; ExF: excitation filter; DM: dichroic mirror; OBJ: objective; PZT-S: piezo-electric translation nano-stage; NF: notch filter; BS: beam splitter; L: lens; PH: pinhole; EmF: emission filter; SPCM: single-photon counting modular; DAQ: data acquisition card; PC: personal computer.

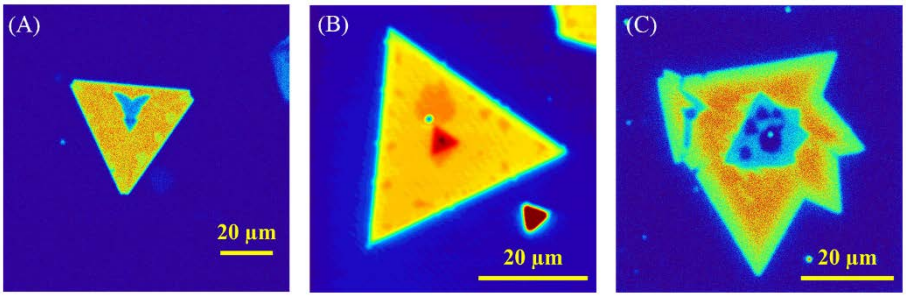

Fig. S3 PL imaging of the prepared WS_2. The inhomogeneous PL intensity indicates the inhomogeneous quality of monolayer WS_2.

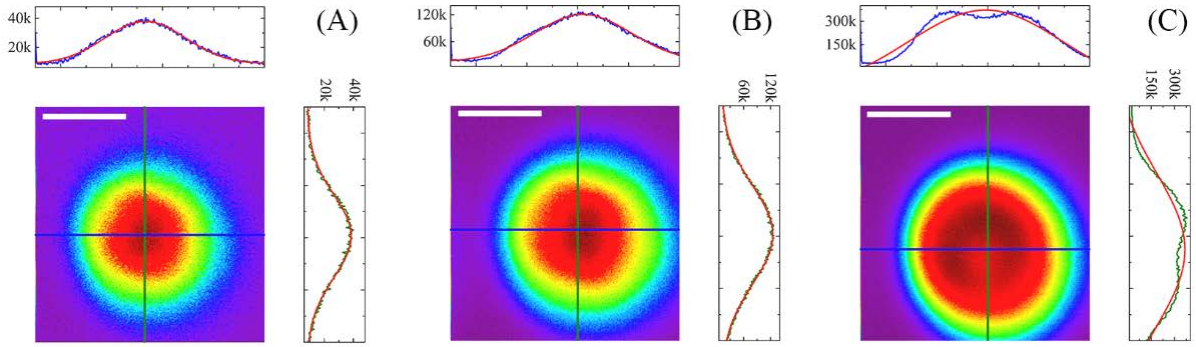

Fig. S4 Profiles of focused laser beam at the power density of 2.1, 7.0, and 15.0 MW/cm^2. The intensity profiles of the highlighted lines are all fitted by Gauss function. Scale bar: 1 μm.

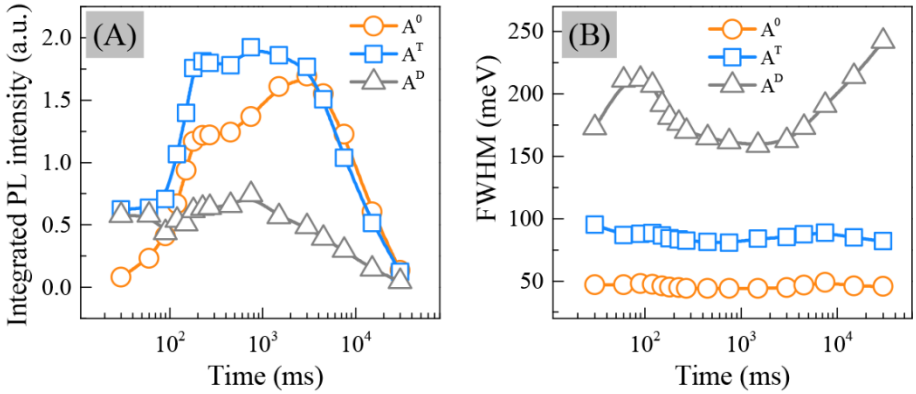

Fig. S5 Time evolution of integrated PL intensities (A) and full width at half maximum (FWHM) (B) of the exciton (A^0), trion (A^T), and defect-bound localized exciton (A^D) as a function of irradiation time (in log scale).

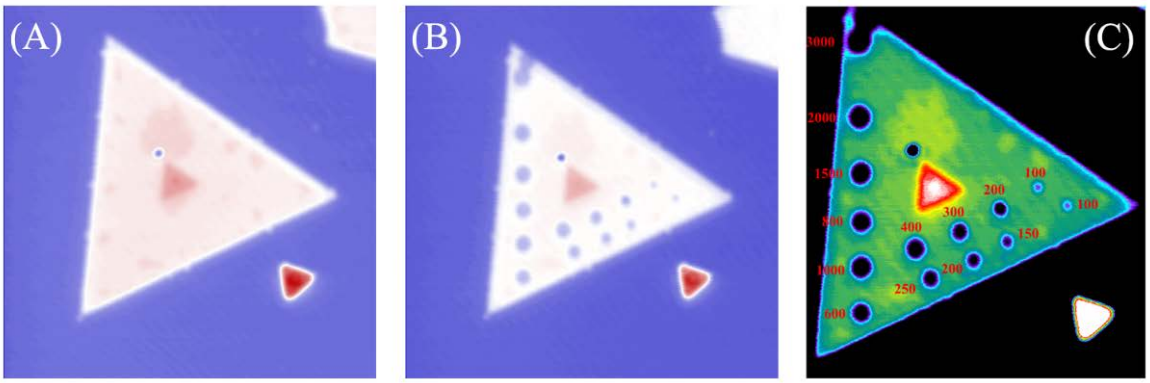

Fig. S6 PL image of the as-prepared (A) and post-engineered (B, C) monolayer WS_2 with different irradiation times (as labeled in C, the unit is ms) under vacuum condition (< 1 Pa). We can find that PL quenching can be observed under all conditions.

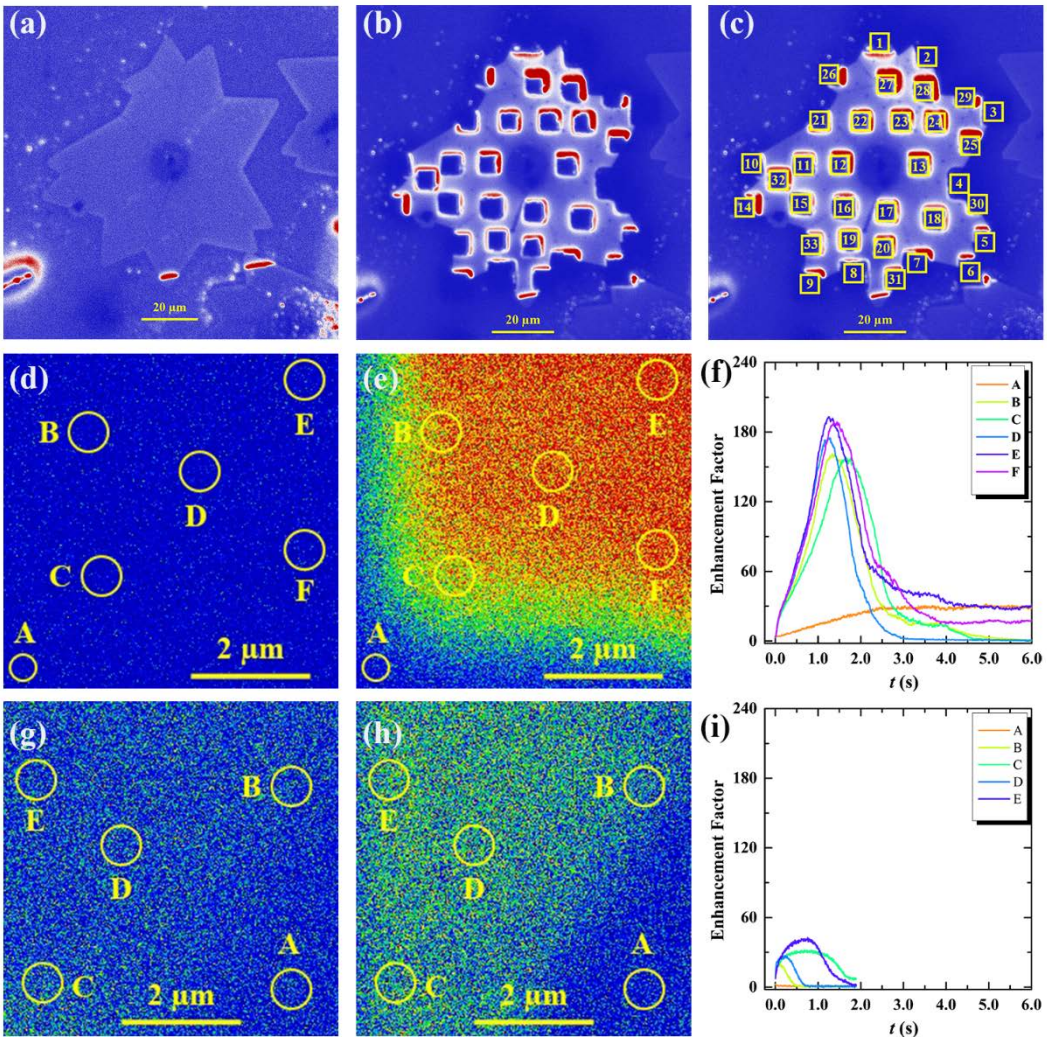

Fig. S7 Power-dependent PL enhancement factor trajectory. PL image of as-prepared (a) and post-engineered (b) monolayer WS_2 with different laser powers. The irradiation area was set as a 4 μm × 4 μm square. The laser power of each engineered area is listed in Table S1; the engineered sequence numbers have been labeled in (c). (d) PL image of the as-prepared sample (No. 11) and (e) the post-engineered area with the power density of 6.95 MW/cm^2 and time of 1.0 s, respectively. (f) PL enhancement factor trajectories of six selected areas, where A-E were used to gain the averaged enhancement factor. (g) PL image of the as-prepared sample (No. 31) and (e) the post-engineered area with the power density of 15.0 MW/cm^2 and time of 0.2 s, respectively. (f) PL enhancement factor trajectories of five selected areas, where A-D was used to gain the averaged enhancement factor.

Table S1 Irradiation powers of each marked area.

No.	Power (mW)	No.	Power (mW)
1	2.1	18	10.0
2	2.1	19	10.0
3	3.0	20	10.0
4	3.0	21	11.0

5	4.0	22	11.0
6	4.0	23	11.0
7	5.0	24	12.0
8	5.0	25	12.0
9	6.0	26	13.0
10	6.0	27	13.0
11	6.9	28	13.0
12	6.9	29	14.0
13	8.0	30	14.0
14	8.0	31	15.0
15	9.0	32	15.0
16	9.0	33	15.0
17	9.0		

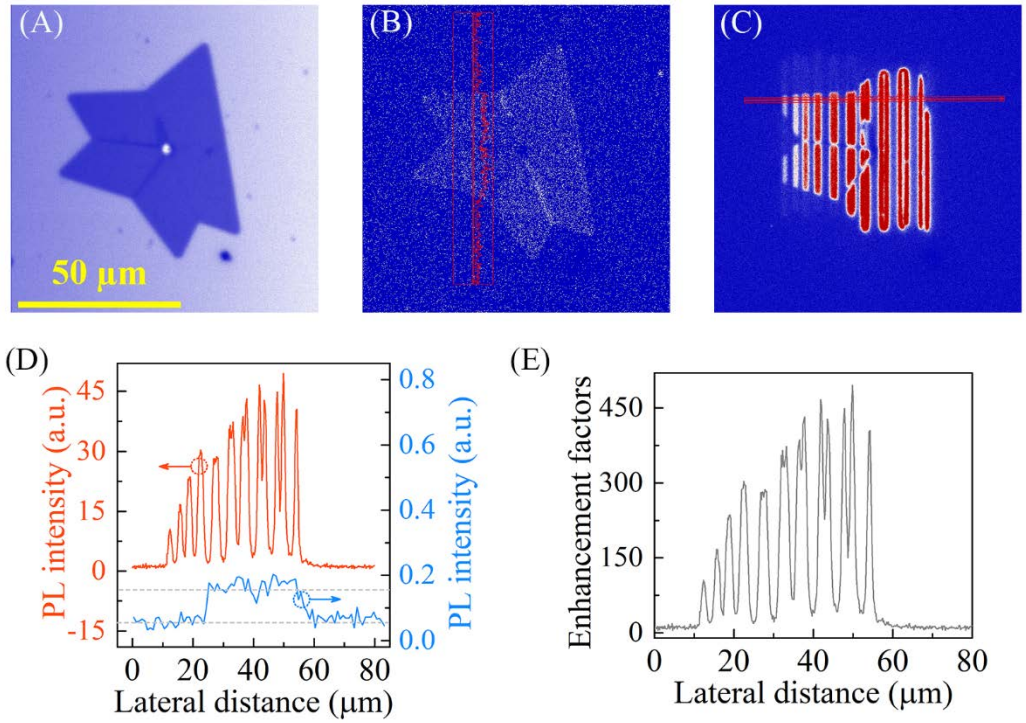

Fig. S8 (A) Reflection image and (B) PL image of as-prepared monolayer WS_2. (C) PL image of post-engineered monolayer WS_2 with the power of 8.3 MW/cm^2 and irradiation time of 1 s. We find that the grain boundary cannot be significantly enhanced. (D) PL intensities along the lines indicated in B and C. (E) Enhancement factor of the post-engineered area shown in C, calculated according to the PL intensity shown in Figure D. The maximum enhancement factor for this monolayer WS_2 can be up to more than 450.

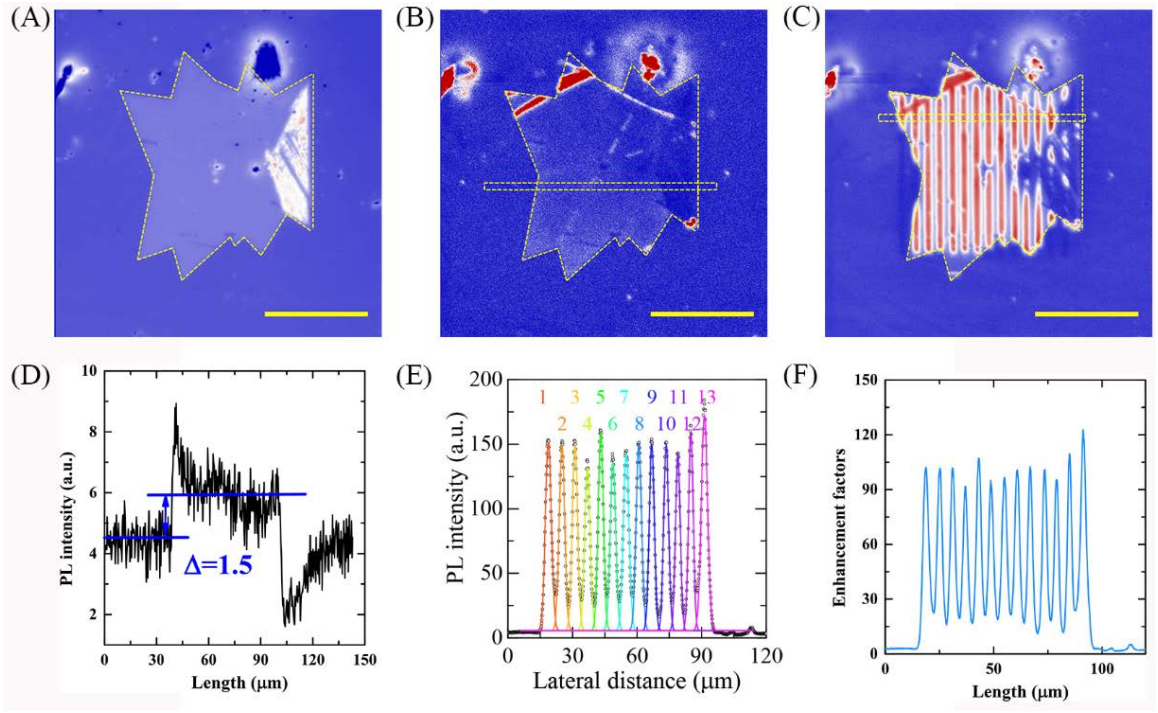

Fig. S9 Reflection image (A), PL image of as-prepared (B), and post-engineered (C) of monolayer WS_2. Scale bar: 50 μm. (D-E) PL intensity profiles along the B and C, respectively. The solid lines in E are the fitting curves by multi-Gauss functions. The fit results are listed in Table S2. (F) PL enhancement factor of the marked area shown in C.

Table S2 Fitted parameters of micro-grating.

No.	FWHM (μm)	Height (a.u.)
1	2.78	146
2	2.57	144
3	2.47	143
4	2.55	126
5	2.47	153
6	2.55	130
7	2.66	137
8	2.54	144
9	2.34	144
10	2.29	144
11	2.19	137
12	2.18	153
13	2.88	166

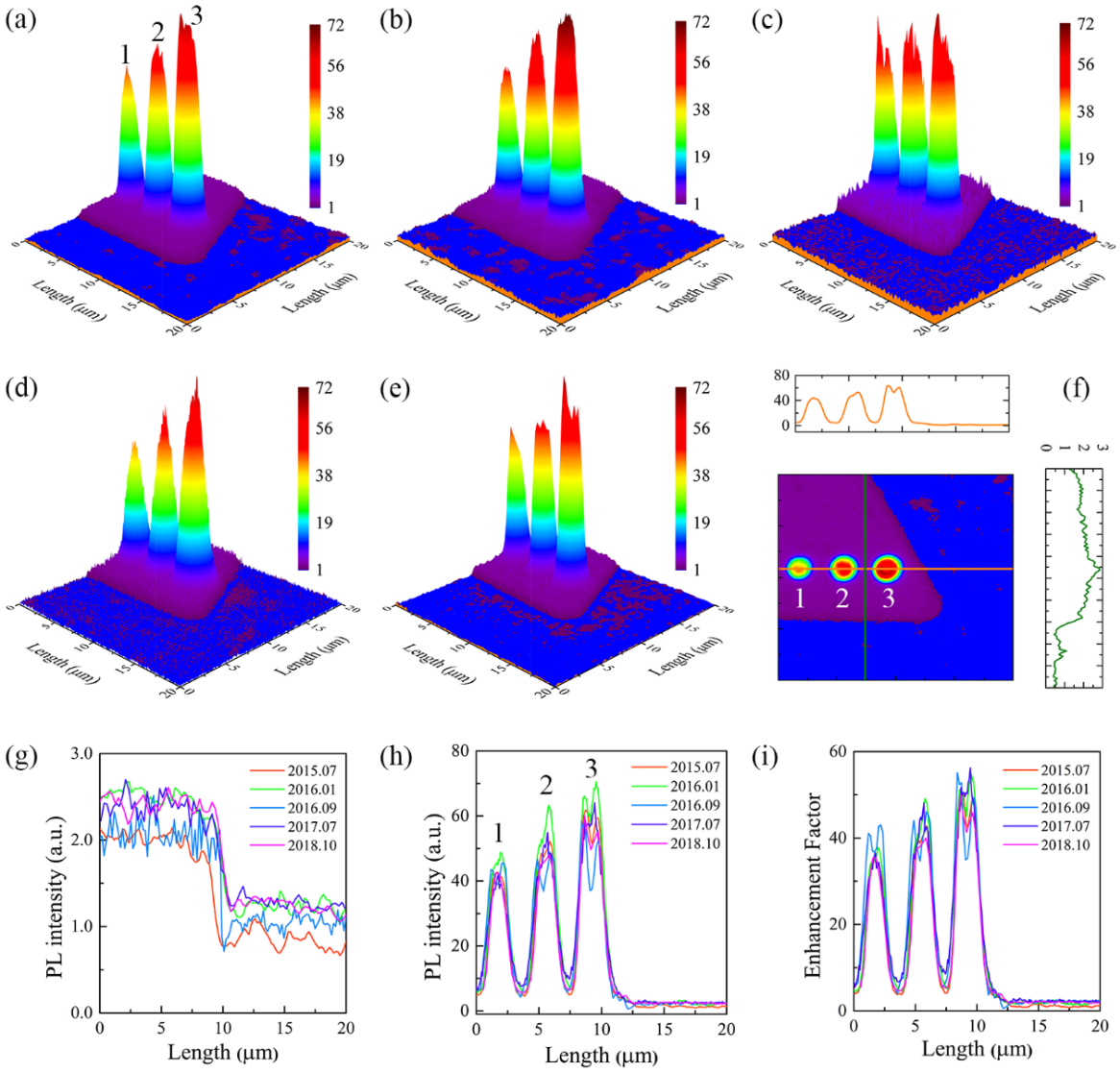

Fig. S10 Robust of the PL enhancement. Three-dimensional PL image of the engineered areas at (a) 2015.07 (first engineered), (b) 2016.01, (c) 2016.09, (d) 2017.07, and (e) 2018.10, respectively. The irradiation laser was femtosecond laser with the power density of 8.3 MW/cm^2. The irradiation times for spots 1, 2, and 3 were 800 ms, 1000 ms, and 1200 ms, respectively. The excitation laser for PL image was 405 nm CW laser with the power density of 0.3 kW/cm^2 and the integrated time for each pixel of 0.01 s. The marked lines (f) and the corresponding PL intensity profiles of the as-prepared sample (g) and the post-engineered sample (h), respectively. (i) The calculated PL enhancement factors.

References

1. Y. Gong, Z. Lin, G. Ye, G. Shi, S. Feng, Y. Lei, A. L. Elías, N. Perea-Lopez, R. Vajtai, H. Terrones, Z. Liu, M. Terrones, and P. M. Ajayan, Tellurium-assisted low-temperature synthesis of MoS_2 and WS_2 monolayers. *Acs Nano* 9, 11658 (2015) https://doi.org/10.1021/acsnano.5b05594

2. M. R. Molas, K. Nogajewski, M. Potemski, and A. Babiński, Raman scattering excitation spectroscopy of monolayer WS_2, *Sci. Rep*. 7, 5036 (2017) https://doi.org/10.1038/s41598-017-05367-0

3. A. Berkdemir, H. R. Gutiérrez, A. R. Botello-Méndez, N. Perea-López, A. L. Elías, C.-I. Chia, B. Wang, V. H. Crespi, F. López-Urías, J.-C. Charlier, H. Terrones, and M. Terrones, Identification of individual and few layers of WS_2 using Raman spectroscopy, *Sci. Rep.* 3, 1755 (2013) https://doi.org/10.1038/srep01755